RSC Advances

PAPER

View Article Online
View Journal | View Issue

Cite this: *RSC Adv.*, 2021, **11**, 18093

Sulfur-inserted polymer-anchored edge exfoliated graphite for durable positive electrodes for lithium–sulfur batteries†

Nanami Uesugi,[a] Natsuho Kazahaya,[a] Koki Yamada,[a] Seiya Kojo,[a] Hiroshi Yoshitani,[b] Takuya Wada,[b] Hiroji Fukui,[b] Shoji Nozato,[b] Yu Katayama *[a] and Hiromori Tsutsumi[a]

Lithium–sulfur batteries hold promising potential for next-generation high-energy-density energy storage. One of their major technical problems is the sulfur active material loss and significant volume change during the charge–discharge process, resulting in rapid capacity fading. Here, we propose sulfur-inserted polymer-anchored edge exfoliated graphite as a positive electrode to accommodate the conflicting requirement of physically restraining sulfur dissolution while maintaining structural flexibility to cope with the volume expansion. The introduction of sulfur between the flexible polymer-anchored graphene layers is achieved by a simple chemical reaction at ambient temperature. The obtained sulfur–carbon composite demonstrates superior sulfur efficiency and cyclability compared to mesoporous carbon-based counterparts. The strong interfacial attraction between sulfur and highly-conductive graphene sheets at the confined interlayer space enables rapid charge transfer and effectively inhibits the polysulfide dissolution, resulting in improved redox reaction reversibility and sulfur efficiency. More importantly, the structural flexibility of layered structure, derived from polymer-anchor, guarantees the stable cycling by accommodating the significant volume expansion of sulfur active materials. Our work provides a simple, proof-of-concept strategy for improving the overall performance of carbon-based positive electrode for Li–S batteries.

Received 15th February 2021
Accepted 26th April 2021

DOI: 10.1039/d1ra01225h

rsc.li/rsc-advances

1. Introduction

Developing rechargeable battery technologies beyond the lithium-ion type is vital to meet the urgent demand for electric vehicles and energy storage systems, coping with long-term sustainability in the energy infrastructure.[1,2] Across the electrode materials reported, elemental sulfur (S_8) offers one of the highest gravimetric capacities, together with large earth-abundance and low cost.[3–8] Lithium–sulfur (Li–S) batteries utilize the reactions between elemental sulfur and metal sulfide, which can store two electrons per sulfur atom, yielding the discharge capacity of 1675 mA h g_{sulfur}^{-1}.[9,10] However, Li–S batteries have encountered several decisive difficulties, including poor cyclability, low specific capacity, and low sulfur efficiency,[11–13] all of which are rooted in the complex sulfur chemistries; (1) low electrical conductivity of S_8 and its discharge product (namely Li_2S),[14,15] (2) dissolution of lithium polysulfide intermediates in the electrolyte,[16,17] and (3) significant volume change of sulfur during the lithiation–delithiation process.[18]

Various strategies have been proposed to tackle these problems of Li–S batteries, including the optimization of either highly-conductive support materials and/or electrolytes, to physically restrain polysulfide dissolution. The physical restraint methods have been pursued by carbon coating on sulfur,[19] utilizing polymeric electrolytes,[20] and designing morphology of carbon.[21,22] Recent studies suggest that the carbon with optimized structure, namely, porous carbon materials, can be one of the most effective and facile candidates to inhibit the polysulfide dissolution.[11,23,24] The advantage of porous carbon materials is derived mainly from its excellent conductivity,[13] large surface area, and substantial adsorption property.[25,26] Various porous carbon–sulfur composites have been reported based on carbon nanotubes,[27] mesoporous carbon,[28,29] graphene,[12,30] and hollow carbon.[31] Although some of the Li–S batteries based on those materials have achieved

[a]*Department of Applied Chemistry, Graduate School of Sciences and Technology for Innovation, Yamaguchi University, Tokiwadai, Ube, 755-8611, Japan. E-mail: yuktym@yamaguchi-u.ac.jp; Tel: +81-(0)836-85-9285*

[b]*Advanced Technology Institute, Corporate R&D Center, Sekisui Chemical Co., Ltd., 2-1 Hyakuyama, Shimamoto-cho, Mishima-gun, Osaka 618-0021, Japan*

† Electronic supplementary information (ESI) available: Electrical conductivity and Brunauer–Emmett–Teller (BET) surface area of KB, G, ExG, and PPG–EExG. Summary of the mass loading of sulfur on the cathode, catalyst loading, and sulfur content calculated from TG curve for the catalyst in this study. Thermogravimetric curves for PPG–EExG and PPG–EExG–S(chem). Gas chromatography-mass spectroscopy (GC-MS) curves for M/S = 64 of pure electrolyte, G–S, G–0.3 M Li_2S_8, and Li_2S_2. Gas chromatography-mass spectroscopy (GC-MS) curves for M/S = 64 of KB–S before and after the initial discharge process. See DOI: 10.1039/d1ra01225h

a superior specific capacity of >1000 mA h g_{sulfur}^{-1}, keeping the initial high specific capacity remains a challenge (see Table S1† for the initial capacity and capacity retention of the state-of-the-art positive electrodes). The main obstacle is to maintain an electrochemically favorable electrode structure during long-term cycling, since the rigid porous structure of carbon cannot accommodate the substantial volume change of sulfur and gradually fracture during the redox process.[12,32] The ideal scenario is that the sulfur should be trapped and bound in confined space within the carbon materials to avoid the polysulfide dissolution while accommodating the significant volume expansion by having certain structural flexibility.

In this study, we validated the above material design strategy by chemically inserting sulfur into the graphene layer, which is anchored by flexible and robust polypropylene glycol (PPG), and used as a positive electrode material for Li–S batteries. We designed an effective strategy for inserting sulfur between the polymer-anchored graphene sheet based on a simple acid–base reaction at ambient temperature. The strong interfacial attraction between sulfur and highly-conductive graphene sheet as well as the structural flexibility of graphene layered structure derived from PPG-anchor were keys to achieve the high initial discharge capacity (1154 mA h g_{sulfur}^{-1}) as well as improved cyclability compared to carbon black-based counterparts. Detailed analysis of the cyclic voltammogram and gas chromatography-mass spectroscopy result revealed the enhanced reversibility of the sulfur redox reaction by short and rapid transport of both electrons and Li-ions at the confined layered structure of the electrode. The substantial improvement in Li–S battery performance confirmed the (electro)chemical and structural stability of the proposed electrode during the cycling, avoiding corrosion and/or rupture by significant volume expansion. The proposed electrode thus meets the conflicting requirement of trapping sulfur within the confined and rigid structure while maintaining certain structural flexibility, which carves out the way for the practical application of Li–S battery technologies.

2. Experimental

2.1 Electrocatalyst preparation

Polymer-anchored edge-exfoliated graphite (polymer-EExG) was synthesized following the previously reported method.[33] Polypropylene glycol (PPG, Sanyo Chemical) and polyethylene glycol (PEG, Sanyo Chemical) were selected as an anchoring polymer and decorated at the edge portion of the expanded graphite (PF8, Toyo Tanso) by radical trapping and subsequent heat treatment. The excess polymer was removed by treated the resultant composite at 500 °C for 120 min.

The mechanically mixed carbon–sulfur composite (denoted as G–S(mix), ExG–S(mix), and PPG–EExG(mix)) was obtained by mixing carbon (graphite (G, Wako Pure Chemicals), exfoliated graphite (ExG, Toyo Carbon), and polymer–EExG) with S_8 (Kishida) in a 1 : 2 weight ratio using a mortar for 10 min.

The simple acid–base reaction between sodium thiosulfate (Wako Pure Chemical) and hydrochloric acid (Wako Pure Chemical) was employed to obtain carbon–sulfur composite.[12,34] The solution containing 0.1 g of carbon (G and ExG), 1.7 g of sodium thiosulfate, and 20 mL of deionized water was mixed with 1.2 mL of hydrochloric acid dropwise at 60 °C and stirred for 5 min. The resulting solid product is then filtered and rinsed with deionized water and dried in vacuum at 60 °C for 12 h. The corresponding polymer-EExG–sulfur composite was synthesized in a similar manner, except for having a pre-dispersion process of ultrasonic dispersion in 10 mL of tetrahydrofuran (THF, Wako Pure Chemical) for 3 h. The dispersed liquid added to the solution consists of 1.6 g of sodium thiosulfate and 10 mL of deionized water. The acid–base reaction was carried out following the procedure described above.

2.2 Characterization methods

The microstructure of the electrocatalysts was analyzed by a scanning electron microscope (SEM, JSM-7600F, JEOL Ltd.) equipped with an energy dispersive X-ray spectrometer (EDS, JMS-7600F, JEOL Ltd.). SEM was performed on an accelerating voltage of 5 kV.

The X-ray diffraction (XRD) patterns of the electrocatalysts were obtained using an X-ray diffractometer (Rigaku Ultima IV) with Cu Kα radiation. Thermogravimetric analysis (TGA) was performed using a Thermo Plus EVO II (Rigaku) from room temperature to 500 °C, at a heating rate of 20 °C min^{-1} under helium atmosphere. Thermal decomposition temperature (T_d) was defined as the temperature at which 5% weight loss took place in TGA. The gas chromatography-mass spectroscopy (GC-MS) of the electrode before and after the galvanostatic measurement was performed on GCMS-QP2010Ultra (Shimadzu). After reaching the end-of-charge potential, the CR2032-type coin cell was immediately disassembled in Ar-filled glovebox and dried in the Ar atmosphere before the measurement.

2.3 Electrochemical methods

The electrochemical behavior of the electrodes was confirmed by galvanostatic measurements and cyclic voltammetry (CV) in two-electrodes cells (CR2032-type coin cells). Cells were assembled in an Ar-filled glovebox and comprised of a Li metal foil (Honjo Metal) as the negative electrode, separated by glass filter separator (Advantec). The positive electrode was obtained by mixing carbon–sulfur composite and sodium alginate (Kishida) in a 10 : 1 weight ratio with ultrapure water. The slurry was further stirred for 15 min, followed by deforming for 3 min by electric mixer (AR-100, Thinky). The resultant slurry was deposited on the carbon paper (TGP-H-060, Toray) and dried at 60 °C for 24 h. Subsequently, positive electrodes were cut into a round with a diameter of 10 mm. Mass loading of sulfur on the cathode and catalyst loading for the electrode used in this study were summarized in Table S4.† 100 μL of electrolyte (1 M lithium bis(trifluoromethanesulfonyl)imide (LiTFSA, Kishida) in a 1 : 1 volume ratio 1,2-dimethoxyethane (DME, Kishida) : 1,3-dioxolane (DOL, Kishida) with 0.1 M $LiNO_3$ (Wako pure Chemicals) additive) was impregnated to the glass filter separator.

Galvanostatic charge–discharge measurements were performed in the potential range of 1.7–3.3 V at 30 °C using an automatic charge/discharge instrument (HJ1001SD8, Hokuto

Denko). Cells were charged at a rate of 0.05C (around 0.065 mA cm^{-2}) for all the electrodes, based on the theoretical capacity calculated based on the mass of sulfur obtained by TG measurement. Specific capacity was calculated based on the mass of sulfur (mA h g_{sulfur}^{-1}) unless otherwise noted. An SP-150 Potentiostat (Bio-Logic) was employed to conduct the cyclic voltammetry (CV) with the CR2032-type coin cell. Lithium metals were used as a counter electrode as well as a quasi-reference electrode. Potential is converted to Li/Li^+ scale (V_{Li}) unless otherwise noted.

3. Results

3.1. Effect of sulfur at the graphite interlayer on Li–S battery performances

Chemical incorporation of sulfur to the polymer-anchored edge-exfoliated graphite (polymer-EExG), based on a simple acid–base reaction, introduces sulfur uniformly into the interlayer space of graphene sheets without bulk sulfur formation (Fig. 1).

Scanning electron microscopy (SEM) image (Fig. 1a) and the corresponding elemental mapping of sulfur (Fig. 1a) from energy dispersive spectrometer (EDS) analysis confirmed that the sulfur uniformly dispersed on the graphene surface with negligible bulk sulfur for all the electrodes tested in this study. The significantly improved dispersion of sulfur was observed for the PPG–EExG–S(chem), reflecting the excellent dispersibility of PPG–EExG in the THF-contained aqueous solution for the sulfur deposition reaction.

The amount of sulfur in G–S(chem), ExG–S(chem), and PPG–EExG–S(chem) electrodes were almost the same (~65 wt%), according to the TG analysis (Fig. 1b). All the electrode showed the weight loss at *ca.* 150 °C, which corresponds to the evaporation of S_8.[35] The onset temperature of the weight loss for PPG–EExG–S(chem) was slightly higher (*ca.* 200 °C) than bare S_8 particle (*ca.* 180 °C) synthesized by the same method (noted as S_8(chem)), which indicates the stabilization of sulfur by the strong interaction with support materials.[36] The slight shift of the evaporation temperature for PPG–EExG–S(chem) thus suggests the introduction of S_8 into more confined spaces, *e.g.*, interlayer space of graphene sheets, where S_8 can strongly interact with graphene due to a short contact distance between the S atoms to the graphene sheet. A similar phenomenon was observed for the thermal decomposition of the polymer anchor, where the PPG anchor showed significantly improved thermal stability up to ~600 °C compared to that of pristine PPG (T_d = 250 °C (ref. 33)) (Fig. S1†). Our hypothesis was supported by the XRD analysis (Fig. 1c), where the diffraction peak corresponds to graphite (002) peak negatively shifted for PPG–EExG–S(chem) compared to G–S(chem) and ExG–S(chem). The decrease in the 2θ value corresponds to the expansion of the average graphene layer distance (calculated from 2θ of (002) peaks by Bragg's equation),[37] indicating the introduction of S_8 into the interlayer space of graphene sheets.

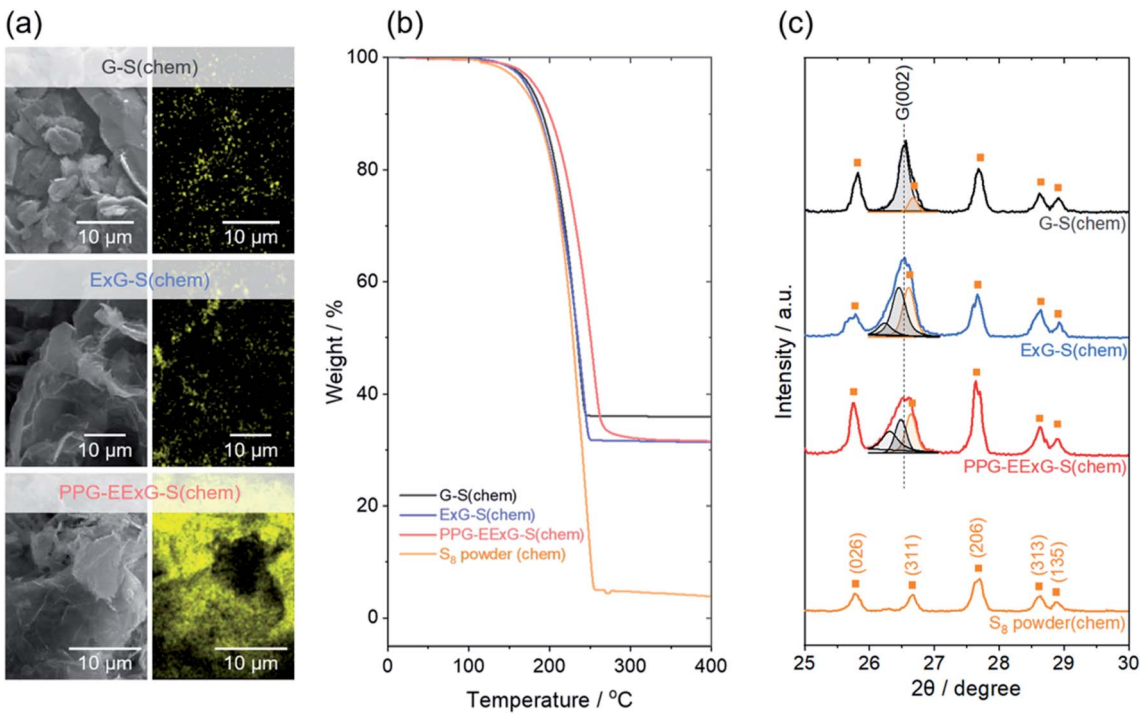

Fig. 1 Characterization of the G–S(chem), ExG–S(chem), and PPG–EExG–S(chem) synthesized *via* chemical incorporation of sulfur. (a) SEM images (left) and corresponding EDS mapping (right) for G–S(chem), ExG–S(chem), and PPG–EExG–S(chem) electrodes. (b) Thermogravimetric curves for G–S(chem), ExG–S(chem), and PPG–EExG–S(chem) obtained under He atmosphere at a heating rate of 20 °C min^{-1}. Thermogravimetric curve for chemically synthesized S_8 powder is also shown for comparison. (c) X-ray diffraction patterns of G–S(chem), ExG–S(chem), and PPG–EExG–S(chem). X-ray diffraction patterns of chemically synthesized S_8 powder is also shown for comparison.

We then evaluated the electrochemical Li storage capability of these carbon–sulfur composites as potential positive electrode materials for Li–S batteries. The PPG–EExG–S(chem) electrode exhibits higher initial capacity as well as cyclability compared with the G–S(chem) and ExG–S(chem), suggesting high sulfur efficiency and less dissolution of intermediates (*e.g.*, polysulfides) for PPG–EExG–S(chem) electrode (Fig. 2). The notable improvement of overall electrochemical performance for the PPG–EExG–S(chem) electrode suggests the critical role of sulfur at the interlayer space of graphene sheets.

Discharge and charge voltage profiles for the carbon–sulfur composites (G–S(chem), ExG–S(chem), and PPG–EExG–S(chem)) containing ~65 wt% sulfur confirms the same pattern of discharge and charge plateaus for all the carbon–sulfur composites at various cycles (Fig. 2a). The discharge curves exhibited typical two-plateau behavior of a sulfur positive electrode, corresponding to the formation of long-chain polysulfides (Li_2S_x, $x > 4$) at 2.3 V and short-chain polysulfides (Li_2S_2 and Li_2S) at 2.1 V.[4,38] Flat plateau for the latter process suggests a uniform deposition of Li_2S with small kinetic barriers.[31] The initial specific capacity (calculated according to the mass of sulfur) was in the order of PPG–EExG–S(chem) (1154 mA h g_{sulfur}^{-1}) > G–S(chem) (876 mA h g_{sulfur}^{-1}) = ExG–S(chem) (870 mA h g_{sulfur}^{-1}), suggesting improved sulfur efficiency for PPG–EExG–S(chem). Furthermore, superior cyclability was confirmed for PPG–EExG–S(chem) electrode compared to the G–S(chem) and ExG–S(chem) electrodes (Fig. 2b). PPG–EExG–S(chem) electrode delivers a reversible capacity of 517 mA h g_{sulfur}^{-1} after 20 cycles with the capacity retention of 45%. The G–S(chem) and ExG–S(chem) electrodes, on the contrary, exhibits a reversible capacity of only 382 mA h g_{sulfur}^{-1} and 374 mA h g_{sulfur}^{-1}, respectively, after 20 cycles. Comparison of the coulombic efficiency also highlights the superior cyclability of PPG–EExG–S(chem) than G–S(chem) and ExG–S(chem), where coulombic efficiency of PPG–EExG–S(chem) showed a steady value of >97.8% after the 10th cycle while that of G–S(chem) and ExG–S(chem) was ~95%. Based on the above experimental findings, we hypothesize that the introduction of sulfur into the interlayer space of graphene sheets plays a pivotal role in the improved initial capacity and cyclability of the PPG–EExG–S(chem) electrode.

Our hypothesis was supported by the evaluation of Li–S battery performance for the corresponding carbon–sulfur composites synthesized *via* mechanical mixing, where no improvement on Li–S battery performance was observed for PPG–EExG-derived electrodes without sulfur at the interlayer space of graphene sheets (Fig. 3).

The XRD patterns of the mechanically mixed carbon–sulfur composites (denoted as G–S(mix), ExG–S(mix), and PPG–EExG–S(mix)) showed negligible change in graphite (002) peak at

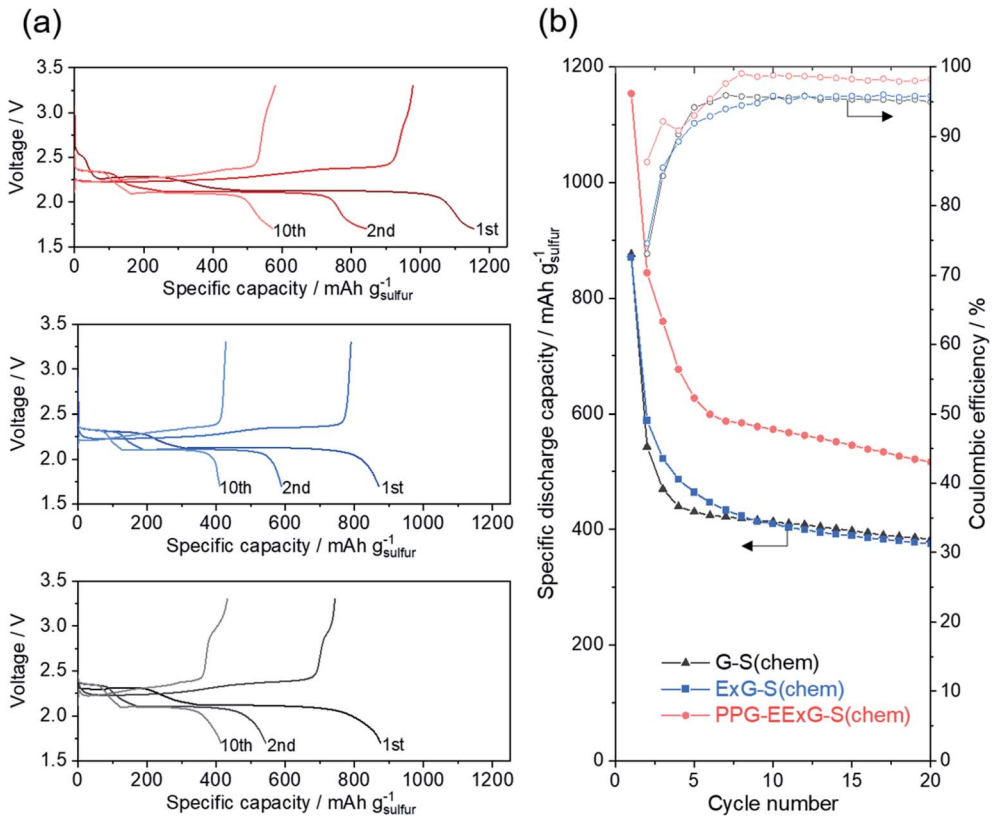

Fig. 2 Electrochemical performance of G–S(chem), ExG–S(chem), and PPG–EExG–S(chem) synthesized *via* chemical incorporation of sulfur. (a) Galvanostatic charge–discharge curves at a rate of 0.05C. Specific capacity was calculated according to the mass of S_8 obtained by TG analysis. (b) Cycle dependence of the specific discharge capacity and coulombic efficiency for G–S(chem), ExG–S(chem), and PPG–EExG–S(chem) electrode calculated from galvanostatic charge–discharge measurement at a rate of 0.05C.

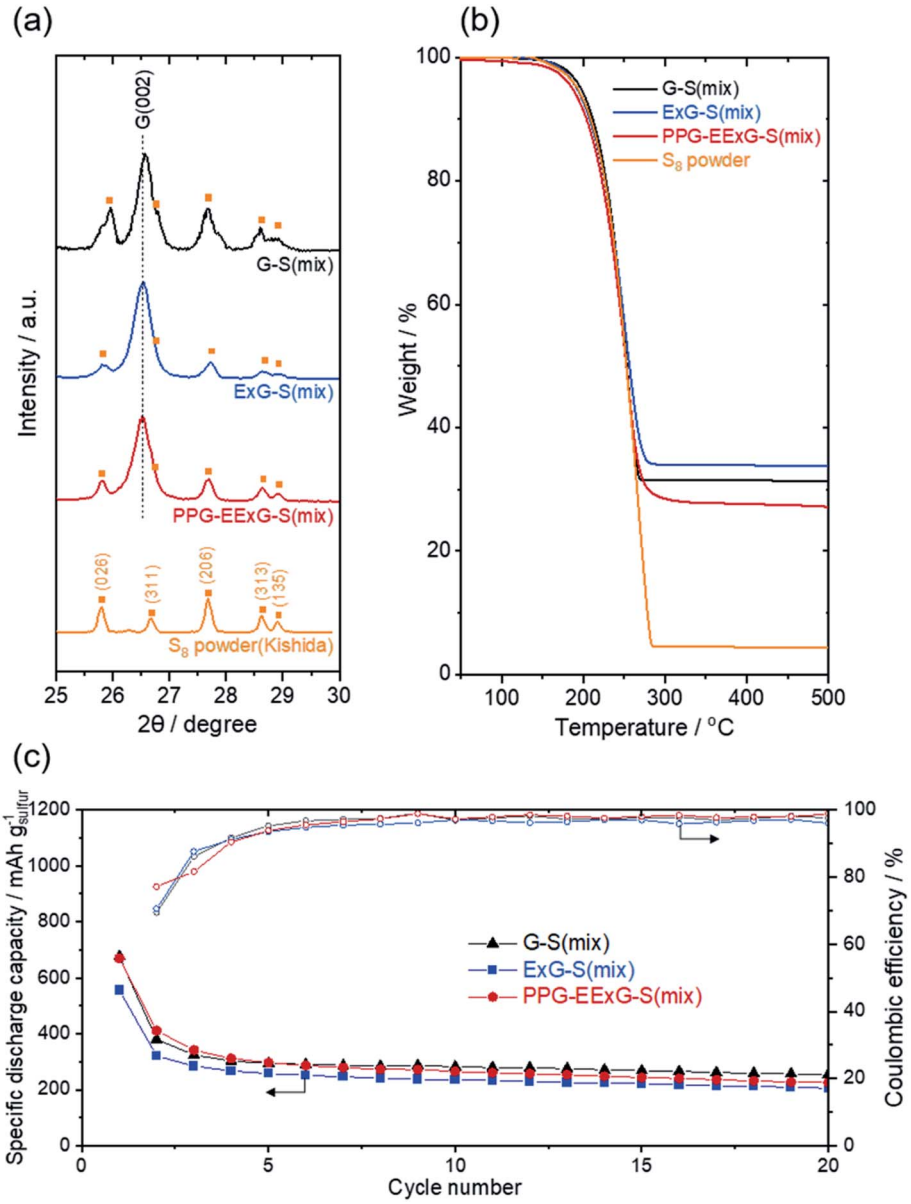

Fig. 3 Characterization and electrochemical performance of the G–S(mix), ExG–S(mix), and PPG–EExG–S(mix) electrodes synthesized *via* mechanical mixing. (a) X-ray diffraction patterns of G–S(mix), ExG–S(mix), and PPG–EExG–S(mix). X-ray diffraction patterns of commercially available S_8 powder is also shown for comparison. (b) Thermogravimetric curves for G–S(mix), ExG–S(mix), and PPG–EExG–S(mix) obtained under He atmosphere at a heating rate of 20 °C min^{-1}. Thermogravimetric curve for commercially available S_8 powder is also shown for comparison. (c) Cycle dependence of the specific discharge capacity and coulombic efficiency for G–S(mix), ExG–S(mix), and PPG–EExG–S(mix) electrode calculated from galvanostatic charge–discharge measurement at a rate of 0.05C.

26.4°, suggesting almost no sulfur was introduced into the interlayer space of graphene sheets *via* mechanical mixing, unlike the chemical incorporation of sulfur (Fig. 3a). Thermogravimetric curves for all the mechanically mixed carbon–sulfur composites overlapped with the TG curve of sulfur powder, further confirms no introduction of sulfur into the interlayer space of graphene occurred *via* mechanical mixing (Fig. 3b). The XRD and TG analysis thus confirm that all the mechanically mixed carbon–sulfur composites, including PPG–EExG–S(mix), have a negligible amount of sulfur at the interlayer space of graphene sheet. Initial specific capacity and cyclability for the G–S(mix), ExG–S(mix), and PPG–EExG–S(mix) electrodes were almost the same (Fig. 3c), indicating the distinctive improvement in initial capacity and cyclability of the PPG–EExG–S(chem) electrode was mainly achieved by the sulfur at the interlayer space of graphene sheet.

3.2. Sulfur redox at the graphite interlayer

In order to understand the details of the sulfur redox reaction at the confined space between the graphene sheet, we compared the electrochemical behavior of PPG–EExG–S(chem) and PEG–EExG–S(chem), having different polymer to anchor the graphene sheet (Fig. 4). The result confirms that the sulfur at graphene interlayer indeed contributes to the high initial

capacity, and preserving the layered structure is the key to the improved cyclability.

We selected two different polymer anchors, PPG and polyethylene glycol (PEG), having slightly different chemical structure to highlight the importance of the polymer anchor and polymer-anchored graphene interlayer on the electrochemical performance. X-ray diffraction pattern confirms the introduction of sulfur into the graphene interlayer for both PPG–EExG–S(chem) and PEG–EExG–S(chem) electrode, suggesting the comparable initial state of the sulfur for those electrodes (Fig. 4a). The shape of graphene (002) peak of PEG–EExG–S(chem) electrode changed significantly after soaked in LiTFSA–DME/DOL electrolyte for 48 h, suggesting the breakage of stacked graphene structure due to the dissolution of PEG-anchor (Fig. 4a). Therefore, PEG–EExG–S(chem) can highlight the effect of the sulfur at the interlayer space on its redox behavior, since it has the sulfur at the graphene interlayer in the beginning, but cannot maintain the stacked graphene structure in the electrochemical condition for a certain time (<48 h). Initial cycle of the cyclic voltammogram was similar for those two electrodes (Fig. 4b); first reduction peak was observed at *ca.* 2.3 V_{Li} followed by the second reduction peak at *ca.* 2.1 V_{Li}, which correlates with the formation of long-chain polysulfides and short-chain polysulfides, respectively. The large oxidation peak corresponds to S_8 formation was observed at *ca.* 2.4 V_{Li}, which gave oxidation current density of 2.5 mA cm^{-2} for PPG–EExG–S(chem) and 2.3 mA cm^{-2} for PEG–EExG–S(chem). The equivalent sulfur redox behavior for PPG–EExG–S(chem) and PEG–EExG–S(chem) electrode in the initial cycle confirms the participation of sulfur at the graphene interlayer in the electrochemical processes, at least in the very beginning.

On the other hand, the cycle dependence of the cyclic voltammogram separates the two electrodes, and only PEG–EExG–S(chem) electrode showed a significant decrease in sulfur redox current by potential cycling (Fig. 4b). Discharge capacity retention, calculated from charge–discharge measurement, was consistent with the cyclic voltammetry, which confirmed the inferior cyclability for PEG–EExG–S(chem) electrode (Fig. 4c). The poor cyclability of the PEG–EExG–S(chem) electrode highlights the crucial role of the graphene interlayer to maintain high capacity. We propose that the strong interfacial attraction between sulfur and graphene at the interlayer, suggested by TG (Fig. 1b), improves the sulfur efficiency and the trapping of sulfur in the confined space inhibits the dissolution and/or diffusion of the polysulfide into the electrolyte. The dissolution of the PEG anchor during the electrochemical measurement gradually ruins the graphene interlayer structure; thus, the large capacity retention was observed for PEG–EExG–S(chem) compared to PPG–EExG–S(chem), while showing the similar sulfur redox behavior in the beginning.

The preferable nature of the polymer-anchored graphene interlayer as a reaction field of a sulfur redox reaction is further clarified by comparing electrochemical performance with conventional carbon–sulfur composite electrode using porous/conductive carbon black (denoted as KB–S(chem)) (Fig. 5). We here propose that the reaction kinetics, as well as the reversibility of the sulfur redox reaction, is enhanced at the polymer-anchored graphene interlayer, due to a short and rapid

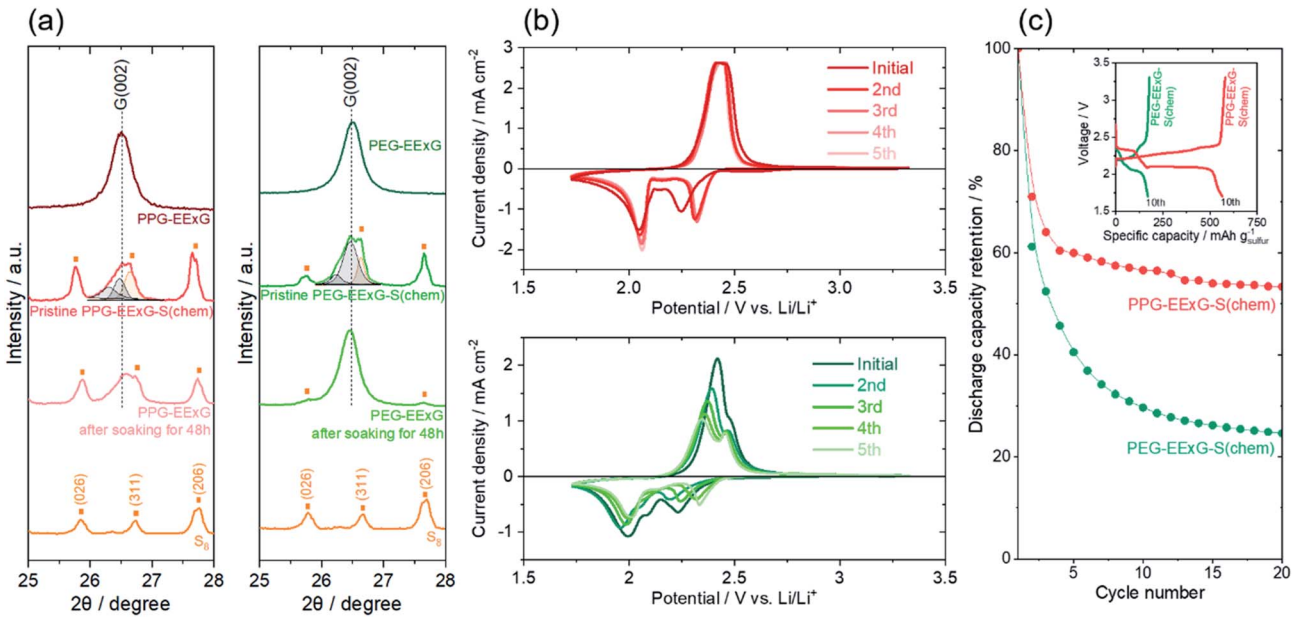

Fig. 4 Comparison between PPG–EExG–S(chem) and PEG–EExG–S(chem) electrodes. (a) X-ray diffraction patterns of PPG–EExG–S(chem) (left) and PEG–EExG–S(chem) (right). X-ray diffraction patterns of chemically synthesized S_8 powder is also shown for comparison. (b) Cyclic voltammograms of PPG–EExG–S(chem) (top) and PEG–EExG–S(chem) (bottom) at a scan rate of 0.1 mV s^{-1}. (c) Cycle dependence of the specific discharge capacity for PPG–EExG–S(chem) and PEG–EExG–S(chem) electrode calculated from galvanostatic charge–discharge measurement at a rate of 0.05C. Inset shows the corresponding charge–discharge curve at 20th cycle.

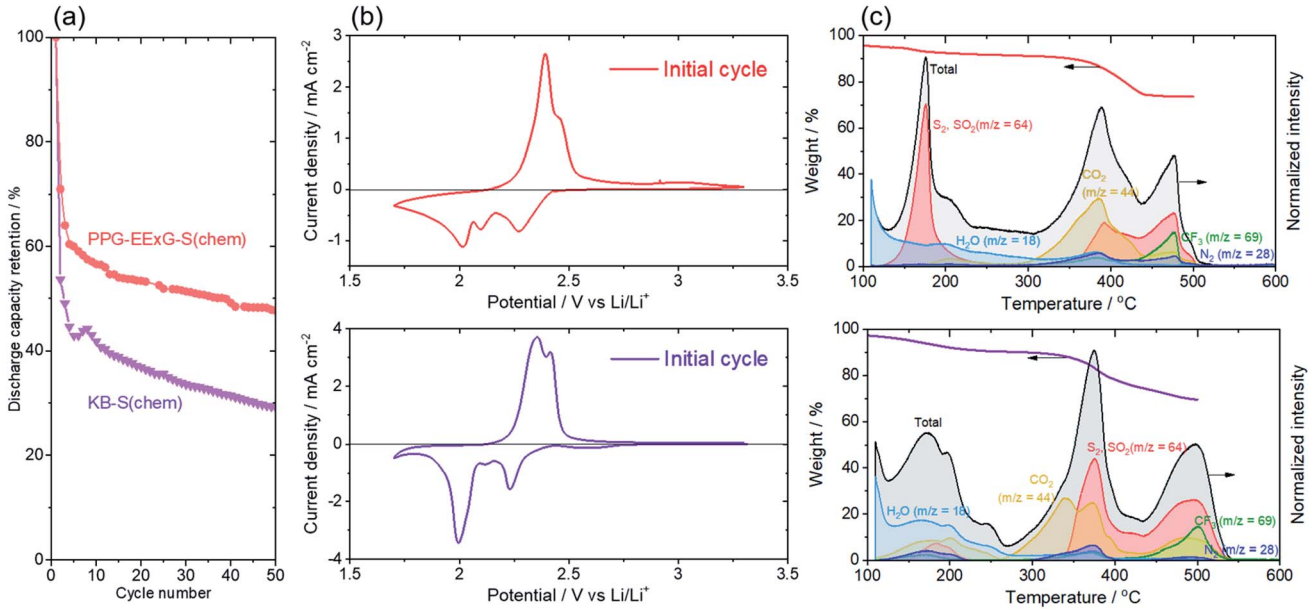

Fig. 5 Comparison between PPG–EExG–S(chem) and KB–S(chem) electrodes. (a) Cycle dependence of the discharge capacity retention for PPG–EExG–S(chem) and KB–S(chem) electrode calculated from galvanostatic charge–discharge measurement at a rate of 0.05C. (b) Cyclic voltammograms of PPG–EExG–S(chem) (top) and KB–S(chem) (bottom) at the initial cycle obtained at a scan rate of 0.1 mV s^{-1}. (c) Gas chromatography-mass spectroscopy (GC-MS) curves for M/S = 64 of PPG–EExG–S(chem) (top) and KB–S(chem) (bottom) after 5th charge of galvanostatic charge–discharge measurement. The corresponding thermogravimetric curve is also shown.

transport pathway for both electrons and Li ions derived from the unique layered structure and its superior electrical conductivity.

The initial discharge capacity of both PPG–EExG–S(chem) and KB–S(chem) showed the similar value (1153 mA h g_{sulfur}^{-1} for PPG–EExG–S(chem) and 1272 mA h g_{sulfur}^{-1} for KB–S(chem)) (Fig. 5a), suggested the high sulfur efficiency accomplished for both electrodes by impregnating sulfur into graphene interlayer and mesopore (2 nm < D < 50 nm),[39,40] respectively, which gave the intimate contact between sulfur and the conductive carbon substrate. However, the significant capacity retention was observed for KB–S(chem) with 37% compared to 45% for PPG–EExG–S(chem) at 20 cycles. One of the reasons for the rapid decrease in KB–S(chem) capacity is the destruction of the mesopores for absorbing the sulfur, which is essential for limiting polysulfide dissolution, due to the significant volume change of sulfur during the redox processes.[41] The PPG–EExG–S(chem), on the other hand, maintains its unique graphene interlayer structure owing to the flexible nature of polymer anchor, which can accommodate the volume expansion of sulfur.

Further detailed analysis of cyclic voltammogram revealed that the reaction reversibility, mainly Li_2S_x (x > 4) ↔ S_8 redox, was improved for PPG–EExG–S(chem) electrode (Fig. 5b). The onset potentials of the first S_8 reduction (S_8 → Li_2S_x (x > 4)) shifted to more positive potential (2.4 V_{Li}) for PPG–EExG–S(chem) than KB–S(chem) (2.3 V_{Li}), suggesting the promotion of the S_8 reduction reaction on PPG–EExG–S(chem). The enhancement of the initial S_8 reduction reaction probably relates to the higher electrical conductivity of the graphene layer (241 S cm^{-1} for PPG–EExG, Table S2†) than the carbon particles (15.2 S cm^{-1} for KB, Table S2†). No potential shift was observed for the subsequent reduction reaction at *ca.* 2.0 V_{Li}, further highlights the contribution of high electrical conductivity on the electrochemical reduction of insulating S_8 particles.

The surface product analysis of the PPG–EExG–S(chem) and KB–S(chem) electrodes after a 5th charge, as deduced from GC-MS experiments, further supports the improved reaction reversibility for PPG–EExG–S(chem) electrode (Fig. 5c). The GC-MS curve of M/S = 64 (corresponds to S_2 and SO_2) clearly showed distinctive features at *ca.* 180 °C, *ca.* 390 °C, and >450 °C, which can be assigned to dissolved S_8, short-chain polysulfides, and TFSI anion, respectively (Fig. S2†). The assignment was further supported by the GC-MS measurement before and after the discharge of KB–S electrode, where a notable decrease of *ca.* 200 °C (S_8) peak was observed along with the increase of *ca.* 390 °C (short-chain polysulfides) peak, suggesting the reduction of S_8 to short-chain polysulfides (Fig. S3†). The intensity ratio of S_8 peak and the peak for short-chain polysulfides was notably larger for PPG–EExG–S(chem) than KB–S(chem), which strongly indicates that more S_8 was formed on the PPG–EExG–S(chem) electrode after a 5th charge. The ex situ reaction product analysis confirms that the PPG–EExG–S(chem) surface is capable of completely oxidize sulfur polysulfides to the last oxidation product (namely S_8) efficiently, even after 5th charge, which can contribute to the improved cyclability of PPG–EExG–S(chem) electrode.

3.3. Mechanistic discussion

We propose that the introduction of sulfur into the interlayer space of graphene sheets plays a pivotal role in the improved

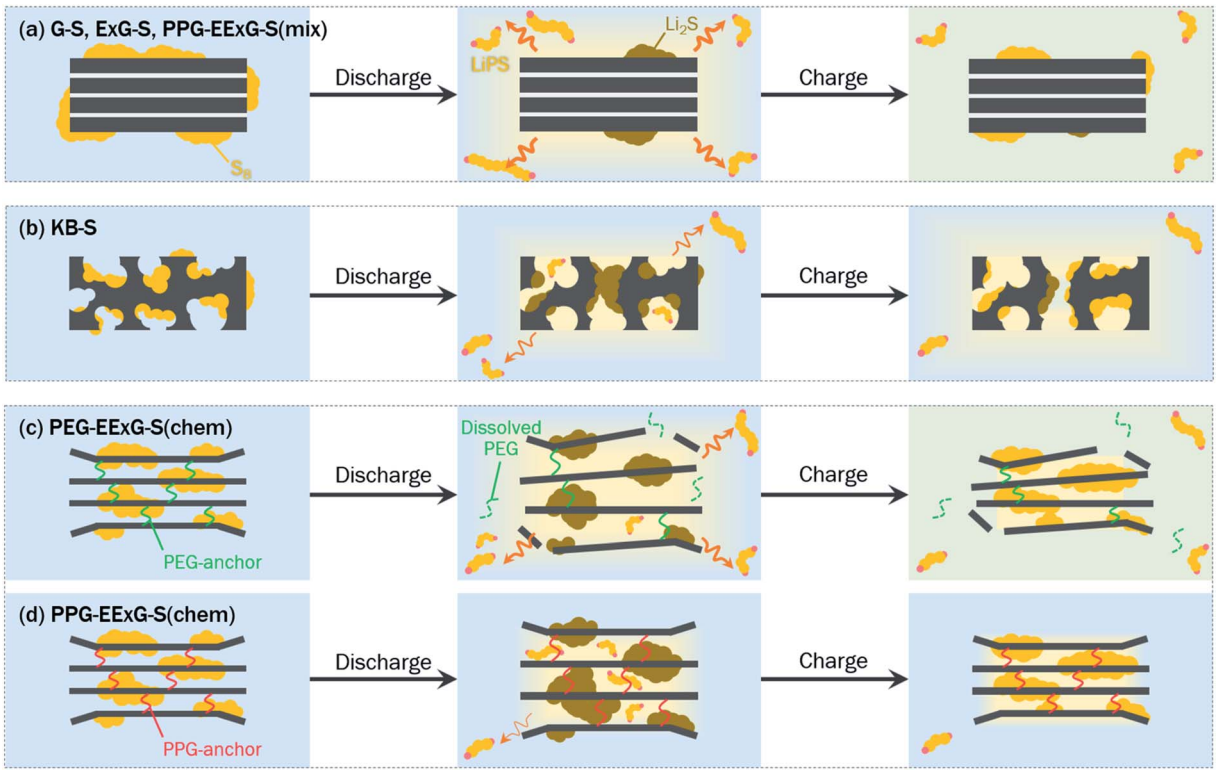

Scheme 1 Comparison of the proposed mechanisms during Li–S battery operation. (a) Proposed mechanisms for G–S, ExG–S, and PPG–EExG–S(mix) electrodes, showing the dissolution and/or diffusion of the lithium polysulfide to the electrolyte. (b) Proposed mechanisms for KB–S(chem) electrode, illustrating the gradual change in the electrode morphology due to the volume expansion of sulfur during charge–discharge. Proposed mechanisms for (c) PEG–EExG–S(chem) and (d) PPG–EExG–S(chem) electrode, where chemically stable and flexible PPG-anchor help maintaining the unique layered structure throughout the Li–S battery operation, resulting the improved initial capacity and cyclability for electrode.

initial capacity and cyclability of the PPG–EExG–S(chem) electrode (Scheme 1).

For G–S, ExG–S, and PPG–EExG–S(mix) electrodes, elemental sulfur is mainly deposited on the surface, not in the graphene interlayer, which cannot promise rapid charge transfer and prevent sulfur being dissolved into the electrolyte (Scheme 1a). Although KB–S(chem) efficiently utilizes the sulfur in the initial discharge owing to its porous structure,[42] the electrode morphology gradually ruins by the significant volume change of sulfur active materials, leading to a considerable decrease in capacity after several cycles (Scheme 1b).

The unique structure of PPG–EExG–S(chem) with superior electrical conductivity of graphene sheets (see Table S2†) provides a short and rapid transport pathway for both electrons and Li ions to achieve improved reaction kinetics (Scheme 1d). The large surface area (see Table S3†), provided by the efficient use of the graphene interlayer, contributes to the intimate contact between sulfur and graphene. Furthermore, sulfur at the interlayer space may possess a strong interfacial attraction between sulfur and graphene due to a short contact distance from the S atoms to the graphene sheet. The strong sulfur–support interaction promises rapid charge transfer and prevents sulfur from being dissolved into the electrolyte. Besides, the polymer anchor, which holds the graphene sheet, provides structural flexibility to accommodate the significant volume changes for sulfur during the redox processes and helps to preserve the morphology of the electrodes. PEG–EExG–S(chem), with chemically unstable PEG-anchor, showed high initial capacity but failed to show the excellent cyclability, mainly due to the destruction of the unique layered structure upon further charge–discharge cycle (Scheme 1c).

4. Conclusions

In summary, a sulfur-inserted polymer-anchored edge exfoliated graphite material (PPG–EExG–S(chem)) was introduced as a positive electrode for lithium–sulfur battery with high discharge capacity as well as improved cyclability. The chemical incorporation based on a simple acid–base reaction enables the insertion of elemental sulfur in the graphene interlayer, anchored by PPG polymer. The strong interfacial attraction between sulfur and highly-conductive graphene sheet at the confined interlayer space enables rapid charge transfer and limits the dissolution of sulfur into the electrolyte, which improves the redox reaction reversibility and sulfur efficiency. The structural flexibility derived from PPG-anchor is a key to maintain the initial capacity over the cycles, by accommodating the significant volume changes of sulfur during the redox processes without destroying the unique structure. The

substantial improvement in lithium–sulfur battery performance by PPG–EExG–S(chem) is thus achieved by the characteristic consistency of sulfur trapping within the confined and rigid structure while having certain structural flexibility to deal with the volume change during the reaction. This work proposes one of the promising design strategies of electrode materials for the next-generation lithium–sulfur batteries, which enables further improvement in the initial capacity as well as the cyclability.

Author contributions

The manuscript was written with contributions from all authors. All authors have approved the final version of the manuscript.

Conflicts of interest

There are no conflicts to declare.

Acknowledgements

This work was supported by Sekisui Chemical Co., Ltd. Part of this work was supported from the Japan Society for the Promotion of Science (JSPS) KAKENHI Grant-in-Aid for Early-Career Scientists under Grant Number 19K15360 (Y. K.).

References

1 M. M. Thackeray, C. Wolverton and E. D. Isaacs, Electrical Energy Storage for Transportation – Approaching the Limits of, and Going beyond, Lithium-Ion Batteries, *Energy Environ. Sci.*, 2012, **5**(7), 7854–7863, DOI: 10.1039/c2ee21892e.

2 M. S. Whittingham, Special Editorial Perspective: Beyond Li-Ion Battery Chemistry, *Chem. Rev.*, 2020, **120**(14), 6328–6330, DOI: 10.1021/acs.chemrev.0c00438.

3 A. Manthiram, Y. Fu, S. H. Chung, C. Zu and Y. S. Su, Rechargeable Lithium–Sulfur Batteries, *Chem. Rev.*, 2014, **114**(23), 11751–11787, DOI: 10.1021/cr500062v.

4 X. Ji and L. F. Nazar, Advances in Li–S Batteries, *J. Mater. Chem.*, 2010, **20**(44), 9821–9826, DOI: 10.1039/b925751a.

5 H.-J. Peng, J.-Q. Huang, X.-B. Cheng and Q. Zhang, Lithium–Sulfur Batteries: Review on High-Loading and High-Energy Lithium–Sulfur Batteries (Adv. Energy Mater. 24/2017), *Adv. Energy Mater.*, 2017, **7**(24), 1770141, DOI: 10.1002/aenm.201770141.

6 P. G. Bruce, S. A. Freunberger, L. J. Hardwick and J. M. Tarascon, LigO_2 and LigS Batteries with High Energy Storage, *Nat. Mater.*, 2012, **11**(1), 19–29, DOI: 10.1038/nmat3191.

7 J. Hassoun and B. Scrosati, Moving to a Solid-State Configuration: A Valid Approach to Making Lithium-Sulfur Batteries Viable for Practical Applications, *Adv. Mater.*, 2010, **22**(45), 5198–5201, DOI: 10.1002/adma.201002584.

8 R. Xu, J. Lu and K. Amine, Progress in Mechanistic Understanding and Characterization Techniques of Li–S Batteries, *Adv. Energy Mater.*, 2015, **5**(16), 1500408, DOI: 10.1002/aenm.201500408.

9 B. L. Ellis, K. T. Lee and L. F. Nazar, Positive Electrode Materials for Li-Ion and Li-Batteries, *Chem. Mater.*, 2010, **22**(3), 691–714, DOI: 10.1021/cm902696j.

10 Y. X. Yin, S. Xin, Y. G. Guo and L. J. Wan, Lithium–Sulfur Batteries: Electrochemistry, Materials, and Prospects, *Angew. Chem., Int. Ed.*, 2013, **52**(50), 13186–13200, DOI: 10.1002/anie.201304762.

11 H. Yao, K. Yan, W. Li, G. Zheng, D. Kong, Z. W. Seh, V. K. Narasimhan, Z. Liang and Y. Cui, Improved Lithium–Sulfur Batteries with a Conductive Coating on the Separator to Prevent the Accumulation of Inactive S-Related Species at the Cathode-Separator Interface, *Energy Environ. Sci.*, 2014, **7**(10), 3381–3390, DOI: 10.1039/c4ee01377h.

12 H. Wang, Y. Yang, Y. Liang, J. T. Robinson, Y. Li, A. Jackson, Y. Cui and H. Dai, Graphene-Wrapped Sulfur Particles as a Rechargeable Lithium–Sulfur Battery Cathode Material with High Capacity and Cycling Stability, *Nano Lett.*, 2011, **11**(7), 2644–2647, DOI: 10.1021/nl200658a.

13 J. Shim, K. A. Striebel and E. Cairns, The Lithium/Sulfur Rechargeable Cell Effects of Electrode Composition and Solvent on Cell Performance, *J. Electrochem. Soc.*, 2002, **149**, A1321–A1325, DOI: 10.1149/1.1503076.

14 S.-E. Cheon, K.-S. Ko, J.-H. Cho, S.-W. Kim, E.-Y. Chin and H.-T. Kim, Rechargeable Lithium Sulfur Battery II. Rate Capability and Cycle Characteristics, *J. Electrochem. Soc.*, 2003, **150**, A800–A805, DOI: 10.1149/1.1571533.

15 C. Barchasz, J.-C. Leprêtre, S. Patoux and F. Alloin, Electrochemical Properties of Ether-Based Electrolytes for Lithium/Sulfur Rechargeable Batteries, *Electrochim. Acta*, 2013, **89**, 737–743, DOI: 10.1016/j.electacta.2012.11.001.

16 R. D. Rauh, K. M. Abraham, G. F. Pearson, J. K. Surprenant and S. B. Brummer, A Lithium/Dissolved Sulfur Battery with an Organic Electrolyte, *J. Electrochem. Soc.*, 1979, **126**(4), 523–527, DOI: 10.1149/1.2129079.

17 Y.-S. Su, Y. Fu, B. Guo, S. Dai and A. Manthiram, Fast, Reversible Lithium Storage with a Sulfur/Long-Chain-Polysulfide Redox Couple, *Chem.–Eur. J.*, 2013, **19**(26), 8621–8626, DOI: 10.1002/chem.201300886.

18 B. Jin, L. Yang, J. Zhang, Y. Cai, J. Zhu, J. Lu, Y. Hou, Q. He, H. Xing, X. Zhan, *et al.*, Bioinspired Binders Actively Controlling Ion Migration and Accommodating Volume Change in High Sulfur Loading Lithium–Sulfur Batteries, *Adv. Energy Mater.*, 2019, **9**(48), 1902938, DOI: 10.1002/aenm.201902938.

19 Y. J. Choi, Y. D. Chung, C. Y. Baek, K. W. Kim, H. J. Ahn and J. H. Ahn, Effects of Carbon Coating on the Electrochemical Properties of Sulfur Cathode for Lithium/Sulfur Cell, *J. Power Sources*, 2008, **184**(2), 548–552, DOI: 10.1016/j.jpowsour.2008.02.053.

20 J. Hassoun and B. Scrosati, A High-Performance Polymer Tin Sulfur Lithium Ion Battery, *Angew. Chem., Int. Ed.*, 2010, **49**(13), 2371–2374, DOI: 10.1002/anie.200907324.

21 Q. Shen, M. Hou, D. Liang, Z. Zhou, X. Li, Z. Shao and B. Yi, Study on the Processes of Start-up and Shutdown in Proton

Exchange Membrane Fuel Cells, *J. Power Sources*, 2009, **189**(2), 1114–1119, DOI: 10.1016/j.jpowsour.2008.12.075.

22 Y. Cao, X. Li, I. A. Aksay, J. Lemmon, Z. Nie, Z. Yang and J. Liu, Sandwich-Type Functionalized Graphene Sheet–Sulfur Nanocomposite for Rechargeable Lithium Batteries, *Phys. Chem. Chem. Phys.*, 2011, **13**(17), 7660–7665, DOI: 10.1039/c0cp02477e.

23 B. Zhang, X. Qin, G. R. Li and X. P. Gao, Enhancement of Long Stability of Sulfur Cathode by Encapsulating Sulfur into Micropores of Carbon Spheres, *Energy Environ. Sci.*, 2010, **3**(10), 1531–1537, DOI: 10.1039/c002639e.

24 N. Jayaprakash, J. Shen, S. S. Moganty, A. Corona and L. A. Archer, Porous Hollow Carbon@sulfur Composites for High-Power Lithium–Sulfur Batteries, *Angew. Chem., Int. Ed.*, 2011, **50**(26), 5904–5908, DOI: 10.1002/anie.201100637.

25 J. L. Wang, J. Yang, J. Xie, N. X. Xu and Y. Li, Sulfur–Carbon Nano-Composite as Cathode for Rechargeable Lithium Battery Based on Gel Electrolyte, *Electrochem. Commun.*, 2002, **4**, 499–502, DOI: 10.1016/S1388-2481(02)00358-2.

26 J. Wang, L. Liu, Z. Ling, J. Yang, C. Wan and C. Jiang, Polymer Lithium Cells with Sulfur Composites as Cathode Materials, *Electrochim. Acta*, 2003, **48**, 1861–1867, DOI: 10.1016/S0013-4686(03)00258-5.

27 L. Yuan, H. Yuan, X. Qiu, L. Chen and W. Zhu, Improvement of Cycle Property of Sulfur-Coated Multi-Walled Carbon Nanotubes Composite Cathode for Lithium/Sulfur Batteries, *J. Power Sources*, 2009, **189**(2), 1141–1146, DOI: 10.1016/j.jpowsour.2008.12.149.

28 G. He, X. Ji and L. Nazar, High "c" Rate Li–S Cathodes: Sulfur Imbibed Bimodal Porous Carbons, *Energy Environ. Sci.*, 2011, **4**(8), 2878–2883, DOI: 10.1039/c1ee01219c.

29 R. Demir-Cakan, M. Morcrette, F. Nouar, C. Davoisne, T. Devic, D. Gonbeau, R. Dominko, C. Serre, G. Férey and J. M. Tarascon, Cathode Composites for Li–S Batteries *via* the Use of Oxygenated Porous Architectures, *J. Am. Chem. Soc.*, 2011, **133**(40), 16154–16160, DOI: 10.1021/ja2062659.

30 S. Evers and L. F. Nazar, Graphene-Enveloped Sulfur in a One Pot Reaction: A Cathode with Good Coulombic Efficiency and High Practical Sulfur Content, *Chem. Commun.*, 2012, **48**(9), 1233–1235, DOI: 10.1039/c2cc16726c.

31 G. Zheng, Y. Yang, J. J. Cha, S. S. Hong and Y. Cui, Hollow Carbon Nanofiber-Encapsulated Sulfur Cathodes for High Specific Capacity Rechargeable Lithium Batteries, *Nano Lett.*, 2011, **11**(10), 4462–4467, DOI: 10.1021/nl2027684.

32 W. Zhou, Y. Yu, H. Chen, F. J. DiSalvo and H. D. Abruña, Yolk–Shell Structure of Polyaniline-Coated Sulfur for Lithium–Sulfur Batteries, *J. Am. Chem. Soc.*, 2013, **135**(44), 16736–16743, DOI: 10.1021/ja409508q.

33 S. Nozato, A. Nakasuga, T. Wada, H. Yoshitani and H. Ihara, Facile Preparation Method for Polymer and Exfoliated Graphite Composites and Their Application as Conduction-Promoting Materials, *RSC Adv.*, 2016, **6**(31), 25776–25779, DOI: 10.1039/c6ra00619a.

34 J. S. Yeon, S. H. Park, J. Suk, H. Lee and H. S. Park, Confinement of Sulfur in the Micropores of Honeycomb-like Carbon Derived from Lignin for Lithium–Sulfur Battery Cathode, *Chem. Eng. J.*, 2020, **382**(July 2019), 122946, DOI: 10.1016/j.cej.2019.122946.

35 N. A. Lange, *Lange's Handbook of Chemistry*, McGraw-Hill, New York, 1985.

36 C. Liang, N. J. Dudney and J. Y. Howe, Hierarchically Structured Sulfur/Carbon Nanocomposite Material for High-Energy Lithium Battery, *Chem. Mater.*, 2009, **21**(19), 4724–4730, DOI: 10.1021/cm902050j.

37 J. S. Park, M. H. Lee, I. Y. Jeon, H. S. Park, J. B. Baek and H. K. Song, Edge-Exfoliated Graphites for Facile Kinetics of Delithiation, *ACS Nano*, 2012, **6**(12), 10770–10775, DOI: 10.1021/nn3050227.

38 J. Kim, D. J. Lee, H. G. Jung, Y. K. Sun, J. Hassoun and B. Scrosati, An Advanced Lithium–Sulfur Battery, *Adv. Funct. Mater.*, 2013, **23**(8), 1076–1080, DOI: 10.1002/adfm.201200689.

39 N. Jiang, G. Jiang, D. Niu, J. Mao, M. Chen, K. Li and Y. Li, Decorating Ketjen Black with Ultra-Small Mo_2C Nanoparticles to Enhance Polysulfides Chemisorption and Redox Kinetics for Lithium–Sulfur Batteries, *J. Energy Chem.*, 2020, **51**, 207–215, DOI: 10.1016/j.jechem.2020.04.008.

40 G. He, C. J. Hart, X. Liang, A. Garsuch and L. F. Nazar, Stable Cycling of a Scalable Graphene-Encapsulated Nanocomposite for Lithium–Sulfur Batteries, *ACS Appl. Mater. Interfaces*, 2014, **6**(14), 10917–10923, DOI: 10.1021/am500632b.

41 R. Demir-Cakan, M. Morcrette, Gangulibabu, A. Guéguen, R. Dedryvère and J. M. Tarascon, Li–S Batteries: Simple Approaches for Superior Performance, *Energy Environ. Sci.*, 2013, **6**(1), 176–182, DOI: 10.1039/c2ee23411d.

42 Z. Li, H. B. Wu and X. W. Lou, Rational Designs and Engineering of Hollow Micro-/Nanostructures as Sulfur Hosts for Advanced Lithium–Sulfur Batteries, *Energy Environ. Sci.*, 2016, **9**(10), 3061–3070, DOI: 10.1039/c6ee02364a.